Frontiers in Bioscience Landmark

Front. Biosci. (Landmark Ed) **2026**; 31(11): 56885
https://doi.org/10.31083/FBL56885

Original Research

Multi-Omics Analysis of Lysosomal Component in Mice With Acute Pancreatitis

Wanlian Li[1,†], Ji-ao Chen[1,†], Tian Sun[1], Juan Xiao[1,2,*]

[1]Guangxi Key Laboratory of Molecular Medicine in Liver Injury and Repair, The First Affiliated Hospital of Guilin Medical University, 541001 Guilin, Guangxi, China
[2]Guangxi Health Commission Key Laboratory of Basic Research in Sphingolipid Metabolism Related Diseases, The First Affiliated Hospital of Guilin Medical University, 541001 Guilin, Guangxi, China
*Correspondence: xiaojuan@glmc.edu.cn (Juan Xiao)
[†]These authors contributed equally.
Academic Editor: Amedeo Amedei
Submitted: 23 March 2026 Revised: 15 September 2026 Accepted: 24 September 2026 Published: 20 November 2026

Abstract

Background: Although lysosomes are known to play crucial roles in the progression of acute pancreatitis (AP), their comprehensive molecular landscape during AP pathogenesis remains largely uncharacterized. **Methods:** An AP model was established in C57BL/6 mice. Lysosomes were subsequently isolated from the pancreas, and their purity was confirmed using western blotting. To systematically characterize changes in lysosomal composition, the purified lysosomes were subjected to integrated proteomic and untargeted metabolomic analyses. Differentially abundant proteins with a false discovery rate ≤0.01, a fold change >1.5 or <1/1.5, and $p < 0.05$ were selected. Differential metabolites were screened via the orthogonal partial least squares discriminant analysis model, using variable importance in projection scores >1 and p-values < 0.05 were chosen. Western blotting, colorimetry and thin layer chromatography were used to further validate selected proteins and metabolites, followed by functional characterization of their roles in AP development and progression. **Results:** Multi-omics profiling identified a total of 1049 differentially abundant proteins (568 downregulated and 481 upregulated) and 438 differentially abundant metabolites (237 upregulated and 201 downregulated) in AP lysosomes, indicating extensive lysosomal reprogramming. Integrated protein–metabolite interaction network analysis revealed several significantly dysregulated functional modules: protein digestion and absorption (nutrient uptake), amino acid biosynthesis (metabolic regulation), Hypoxia-Inducible Factor 1 (HIF-1) and sphingolipid signaling pathways (signal transduction), polyamine metabolism and ferroptosis (cell fate determination), and lysosome and phagosome pathway (transport and catabolism). Key molecular changes were validated, including significantly increased levels of Leukemia inhibitory factor (Lif) and Sphingosine kinase 1 (Sphk1) proteins and N1-acetylspermidine in AP lysosomes. In contrast, levels of CXXC-type zinc finger protein 5 (Cxxc5) protein and NAD^+ were significantly decreased. Furthermore, N1-acetylspermidine was found to induce pancreatic injury in mice through a ferroptosis-associated process. **Conclusion:** Lysosome-associated metabolic reprogramming, altered signal transduction, and changes in cell death regulatory pathways occur during AP development.

Keywords: pancreatitis; lysosomes; proteomics; metabolomics

1. Introduction

Characterized by the autodigestion of pancreatic tissue resulting from various etiological factors, acute pancreatitis (AP) is a prevalent gastrointestinal disorder with potentially fatal outcomes. Clinically, AP presents with pancreatic edema, necrosis, hemorrhage, and elevated serum levels of digestive enzymes such as amylase and lipase [1]. The annual incidence of AP worldwide is in the range of 130,000–450,000 cases, with 80%–85% classified as mild-to-moderate and the remaining 15%–20% progressing to severe AP (SAP). The occurrence of systemic inflammatory response syndrome and multiple organ dysfunction syndrome in SAP contributes to its high fatality rate of 13%–35% [2]. With the underlying mechanisms of AP remaining insufficiently elucidated, current clinical interventions are predominantly supportive [3].

The pathogenic cascade of AP involves lysosomes. In these membrane-bound acidic organelles, macromolecular catabolism of proteins, nucleic acids, and polysaccharides occurs [4]. As a result, lysosomes are considered the central regulators of nutrient flux and cellular homeostasis [5]. Furthermore, they are crucial for AP progression, directly modulating disease severity [6]. The genetic ablation of lysosome-associated membrane protein 2 (LAMP-2) disrupts autophagosome–lysosome fusion, thereby triggering cathepsin-mediated autodigestion and acinar cell injury, a pathological phenotype in cerulein-induced AP models [7]. In addition, lysosomal impairment is associated with reduced protease activation and dysregulated membrane trafficking in AP [8]. Nevertheless, the relationship between lysosomal destabilization and AP pathogenesis is not yet fully understood.

Multi-omics approaches in disease research have increasingly been applied in recent years [9,10,11,12]. Strate-

Copyright: © 2026 The Author(s). Published by IMR Press.
This is an open access article under the CC BY 4.0 license.

Publisher's Note: IMR Press stays neutral with regard to jurisdictional claims in published maps and institutional affiliations.

gies integrating temporal proteomics and lipidomics have detected abundant dysregulated metabolites and proteins in cerulein-induced murine AP models [13]. Coupled proteomic/phosphoproteomic profiling has revealed perturbations in oxidative phosphorylation and spliceosome pathways in AP model mice [14]. Clinical cohort analyses have identified four metabolites that were significantly elevated in patients with mild AP compared with healthy controls and decreased after treatment [15]. Furthermore, targeted metabolomic analysis of plasma from patients with AP has identified differentially abundant metabolites between SAP and non-SAP cases, which may serve as potential early prognostic biomarkers [16]. However, current evidence largely focuses on whole-cell analyses of blood or pancreatic tissue [17,18]. Considering the critical roles lysosomes play in AP pathogenesis, in this study, we investigated pancreatic lysosome-specific protein and metabolite profiles through integrated proteomic/metabolomics.

2. Materials and Methods

2.1 Reagents and Antibodies

All chemical reagents used in this study were of analytical grade or higher purity. Tris-base (A501492-0500), glycine (A502065-0500), Acryl/Bis 30% Solution (29:1, B546017-0500), 4× Tris-HCl-SDS separation gel buffer (pH 8.8, C526033-0001), and 4× Tris-HCl-SDS stacking gel buffer (pH 6.8, C526034-0001) were obtained from Sangon Biotech. Cerulein (HY-A0190) was purchased from MedChemExpress. Amylase (105-000475-00), and LDH assay kits were acquired from Mindray. The primary antibodies LAMP1 (D2D11, dilution 1:1000), Sat1 (D1T7M, dilution 1:1000), Bcl2 (D55G8, dilution 1:1000), and Bax (D2E11, dilution 1:1000) were obtained from Cell Signaling Technology; Calnexin (ET1611-86, dilution 1:1000) from HUABIO; Sphk1 (ab71700, dilution 1:1000); GPX4 (ab126066, dilution 1:200) and xCT (ab175186, dilution 1:1000), Goat Anti-Rabbit IgG H&L (Alexa Fluor® 488, dilution 1:200) antibodies from Abcam; COX IV antibody (AG8011, dilution 1:1000) from Beyotime; Cxxc5 (D122172, dilution 1:500 in in western blotting, 1:50 in immunofluorescence) and β-actin (D191047, dilution 1:3000) antibodies from Sangon Biotech; Lif antibody (26757-1-AP, dilution 1:500) from Proteintech; and LC3B antibody (A19665, dilution 1:1000) from ABclonal. N1-acetylspermidine hydrochloride (T37170) was purchased from TargetMol. Dansyl chloride (D823201), cyclohexane (C804201), and L-proline (L816039) were obtained from Macklin. The NAD^+/NADH Assay Kit (S0175) was procured from Beyotime. TLC silica gel plates (HSGF254) were purchased from Yantai Jiangyou Silica Gel Development, while the Iron Stain Kit (DTD04) was obtained from DeepMind.

2.2 Animal Experiments

A total of 86 male wild-type C57BL/6 mice (10–12 weeks old, 22 ± 2 g) were supplied by Hangzhou Ziyuan Experimental Animal Technology Co., Ltd. Mice were maintained under specific pathogen-free conditions at 23 °C ± 1 °C and 60% ± 5% relative humidity with 12-h light/dark cycles, with ad libitum access to food and water. Age- and sex-matched mice were randomized as previously described [19]. For cerulein-induced AP, mice were fasted for 12 h and received hourly intraperitoneal injections of 50 μg/kg cerulein (seven doses in total), while saline-injected mice served as controls. For the N1-acetylspermidine (N1-AcSpd; 5 or 10 mg/kg) treatment, experimental mice were administered a single intraperitoneal injection and euthanized 10 h after injection for serum/pancreatic tissue collection, whereas controls received an equivalent volume of saline. The packaging of the injected drug and the control reagent is exactly the same. Serum samples were centrifuged at 3000 ×g for 15 min (4 °C), and the resulting supernatants were used for analysis. Pancreatic tissues were either fixed in paraformaldehyde (PFA) solution (P1110, Solarbio) for paraffin embedding or flash-frozen in liquid nitrogen for storage at −80 °C. All of the mice in each experiment were included in the final analysis. Administration and measurement are performed by different personnel, with the measurer blinded to group allocation. The study was carried out in accordance with the ARRIVE guidelines.

2.3 Euthanasia

Mice were euthanized using an overdose of isoflurane (Jiangsu H.F.Q Bio-Technology Co., Ltd.) inhalation anesthesia. Briefly, mice were anesthetized with a 5% isoflurane–oxygen mixture, followed by euthanasia via cervical dislocation after the anesthesia took effect.

2.4 Biochemical Analysis

Serum or cell medium samples were diluted at 1:10/1:5 and analyzed for amylase and LDH activities using an automated biochemistry analyzer (Mindray).

2.5 Hematoxylin and Eosin (H&E) Staining

Pancreatic tissues were fixed in 4% PFA and dehydrated through a graded ethanol series. After xylene clearing and paraffin infiltration, serial 5-μm sections were microtome-prepared and stained with H&E (Servicebio) following standard histopathological protocols. The pathological scores were analyzed according to previously published methods [20].

2.6 Transmission Electron Microscopy (TEM)

Pancreatic tissues were fixed in ice-cold 2.5% glutaraldehyde/0.1 M phosphate buffer (pH 7.4) for 2 h. The tissues were then fixed in 1% osmium tetroxide for 1.5 h, followed by dehydration through a graded ethanol-acetone series and embedding in Epon 812 resin. Ultrathin sections

(70 nm) generated via a Leica EM UC7 ultramicrotome were incubated with uranyl acetate/lead citrate and imaged using a Hitachi HT7700 TEM. Four random fields per sample were subjected to semi-quantitative analysis for lysosomal number and maximal diameter in individual acinar cells using ImageJ (National Institute of Health, Bethesda, Maryland, USA).

2.7 Western Blotting

Pancreatic tissue protein extracts were separated via Sodium Dodecyl Sulfate Polyacrylamide Gel Electrophoresis and transferred to Polyvinylidene fluoride membranes (Millipore). The membranes were blocked with 5% skim milk, probed overnight at 4 °C with primary antibodies, and subsequently incubated for 1 h at room temperature with horseradish peroxidase-conjugated secondary antibodies. Anti-mouse IgG, HRP-linked Antibody (Cell Signaling Technology, 7076P2, dilution 1:2000), HRP-conjugated Goat Anti-Rabbit IgG (Sangon Biotech, D110058, dilution 1:2000). Protein bands were visualized using an enhanced chemiluminescence substrate.

2.8 Extraction of Lysosomes From Pancreatic Tissues

Lysosomes were isolated from mouse pancreatic tissues using a Lysosome Isolation Kit (Sigma-Aldrich, LYSISO1) according to the manufacturer's instructions. Pancreatic homogenates in extraction buffer were centrifuged at low speed (1000 ×g, 10 min, 4 °C) to remove debris. The supernatant was subjected to ultracentrifugation (20,000 ×g, 30 min, 4 °C) to pellet organelle-enriched fractions. To selectively induce lysosomal release, pellets were resuspended in 8 mM $CaCl_2$ (final concentration) at 37 °C for 10 min, after which they were centrifuged (5000 ×g, 10 min, 4 °C) to obtain lysosome-enriched supernatants.

2.9 Lysosomal Proteomic Analysis of Pancreatic Tissues

Lysosomal proteomic analysis of mouse pancreatic tissues was performed by Bioprofile Biotechnology (Shanghai). Protein extracts were enzymatically digested and analyzed via Liquid Chromatography-Tandem Mass Spectrometry (LC-MS/MS) in data-independent acquisition (DIA) mode. For DIA-based protein identification and quantification, raw data were processed using DIA-NN against the UniProtKB *Mus musculus* database (Release 2024_12; 87,491 entries).

2.10 Lysosomal Untargeted Metabolomic Analysis of Pancreatic Tissues

Lysosomal untargeted metabolomic analysis of mouse pancreatic tissues was carried out by Bioprofile Biotechnology (Shanghai). Metabolites were obtained from lysosomal fractions and profiled using ultra-performance liquid chromatography–quadrupole time-of-flight mass spectrometry (UPLC-Q-TOF-MS) in data-dependent acquisition (DDA) mode. After quality control, data were annotated against the Human Metabolome Database (HMDB), MassBank, the Global Natural Products Social Molecular Networking (GNPS), and Bioprofile's BP-DB for qualitative analysis.

2.11 Thin Layer Chromatography (TLC) Analysis of -N1-AcSpd

Lysosomal proteins were removed after treatment with acetonitrile–Na_2SO_4 [21]. Metabolites were derivatized with dansyl chloride [22], spotted onto TLC plates, and separated in chambers saturated with ethyl acetate in a single run. The separated metabolites were visualized under UV light.

2.12 NAD^+ Detection Using Colorimetry

NAD^+ content was determined using the Beyotime NAD^+/NADH Assay Kit (WST-8 method, Cat. No. S0175) following the manufacturer's protocol. Samples were diluted to appropriate concentrations, and the diluted samples (with or without 60 °C water bath pretreatment) were mixed thoroughly with the WST-8 reaction system. After 30 min of light-protected incubation at 37 °C, the absorbance at 450 nm was measured, and NAD^+ concentration was calculated via the pre-established standard curve.

2.13 Primary Acinar Cell Isolation, Cultivation, and Processing

Primary acinar cell isolation was from C57BL/6 mice, performed in a sterile environment. Minced pancreatic tissues were subjected to collagenase digestion (37 °C), and the resulting cell suspensions were cultured in DMEM/20% fetal bovine serum (FBS). Purified cells were seeded directly on indicated culture plates for each experiment after isolation, whereas additional digestion is not applicable. Acinar cells were cultured and then treated with 100 μM N1-AcSpd with or without 10 μM Ferrostatin-1 (F864515, MACKLIN) for 2 h. All primary cells were validated for their identity by pancreatic acinar cell marker analysis using immune fluorescence and tested negative for mycoplasma (**Supplementary Fig. 1**).

2.14 Lipid Peroxidation Detection

Detection of lipid peroxidation in primary acinar cells was performed using the commercial C11-BODIPY 581/591 probe (B3930, Solarbio). In brief, after the cells were washed with phosphate buffered saline, the probe was added at 37 °C for 30 min. Subsequently, the solution was removed, cells were washed twice with phosphate buffered saline, and imaged using a fluorescence microscope. The fluorescence signal was quantitatively analyzed using ImageJ.

2.15 Cellular Immunofluorescence

Co-localization of lysosomes with the target proteins was performed in primary acinar cells under the indicated

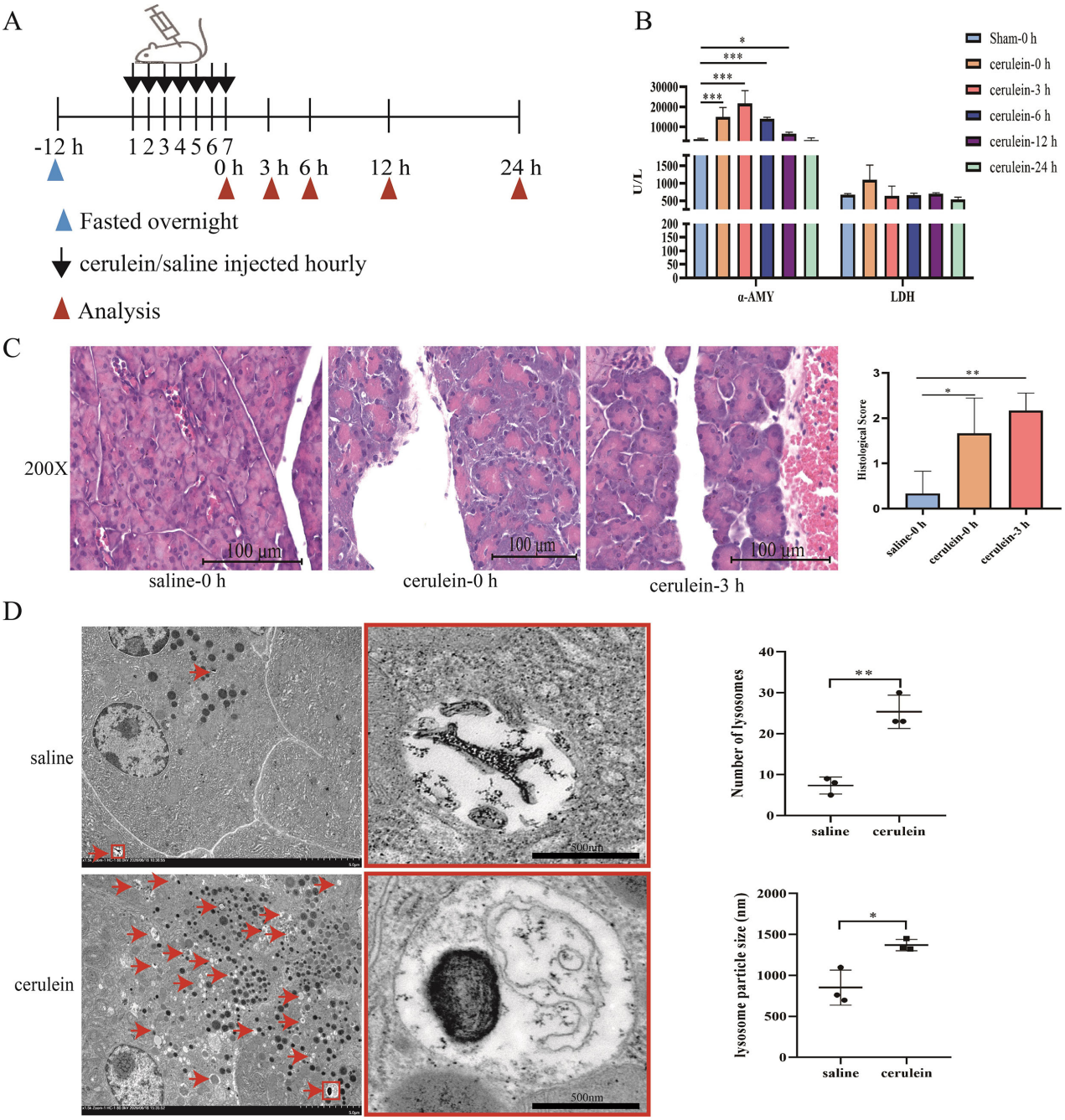


Fig. 1. The establishment of an acute pancreatitis model in mice using cerulein (n = 3 per group). (A) Schematic diagram of cerulein-induced acute pancreatitis (AP) model in mice. (B) Biochemical analysis of serum from AP mice collected at indicated time points after the final injection of cerulein. (C) Hematoxylin and eosin (H&E) staining images of pancreas from AP mice collected at the indicated the time points after the final injection of cerulein, along with the corresponding pancreatic histopathological scores. Scale bar: 100 μm. (D) Representative images of the observed lysosomes. Numbers of structurally intact acinar cells: saline (13, 16, 16), cerulein (7, 7, 10), three fields per sample. Scale bar in the left panel is 5 μm, lysosomes are indicated by red arrows, and magnified views of the regions outlined by red boxes are displayed in the corresponding right panel. Scale bar: 500 nm. The graph represented as Mean ± SD. Significant differences between the two groups were analyzed using Student's *t*-tests. Significant differences among more than two groups were analyzed using analysis of variance (ANOVA). * $p < 0.05$, ** $p < 0.01$, *** $p < 0.001$. There were no exclusions in animals.

treatments. Cells were incubated with 1:200 diluted Lyso-Tracker Red (C1046, Beyotime) at 37 °C for 1 h. The samples were then fixed in PFA, blocked with blocking buffer, and incubated overnight at 4 °C with CXXC-type zinc finger protein 5 (Cxxc5) antibody (1:50 dilution). Following treatment with the corresponding fluorescent secondary an-

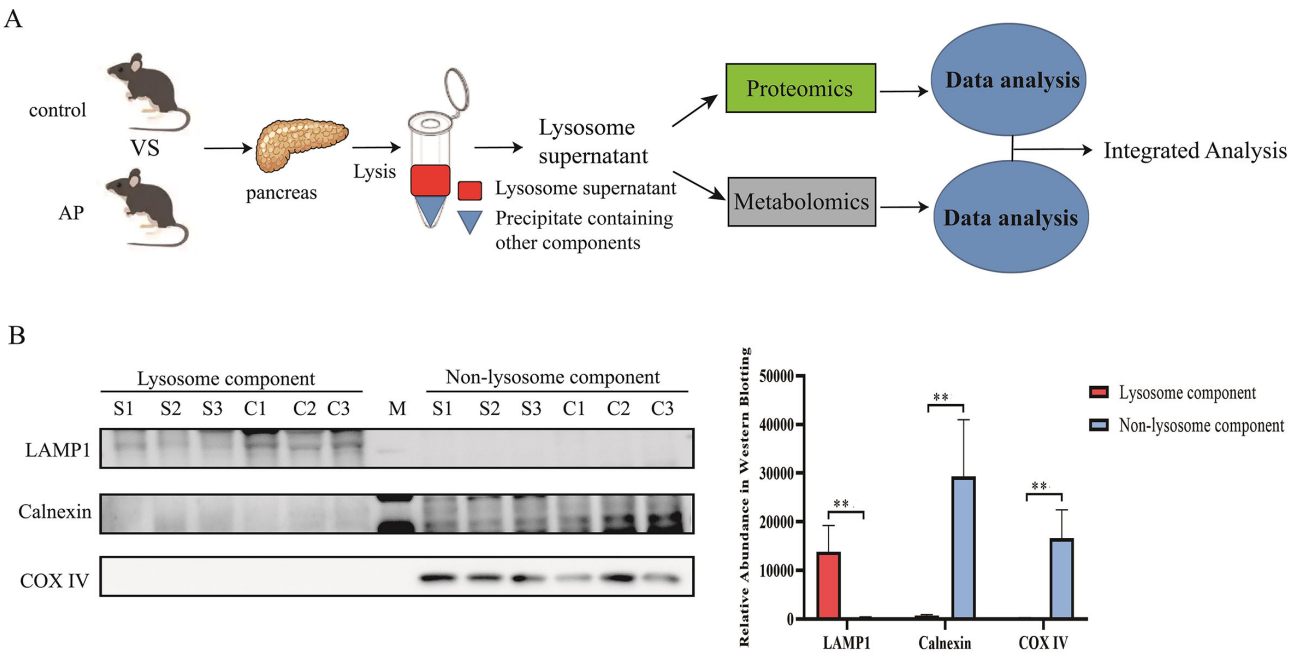


Fig. 2. Lysosome extraction. (A) Workflow for lysosomes from the pancreas of mice for proteomics and metabolomics (n = 3 per group). (B) Indicated lysosome components were analyzed by western blotting with indicated antibodies (M, Protein Marker; LAMP1, lysosome-associated membrane protein 1; Calnexin, Calcium-binding protein, endoplasmic reticulum; COX IV, cytochrome c oxidase IV; mitochondrion, n = 3 per group). Significant differences between the two groups were analyzed using Student's *t*-tests. ** $p < 0.01$. There were no exclusions in animals.

tibody, nuclei were stained with DAPI. Finally, fluorescence images were captured using a fluorescence microscope.

2.16 Statistical Analysis

Differentially abundant proteins or metabolites were identified, and significant differences between the two groups were analyzed using Student's *t*-tests ($p < 0.05$). Significant differences among more than two groups were analyzed using one-way analysis of variance (ANOVA). Statistical analyses (Student's *t*-test and one-way ANOVA) were performed using SPSS 19.0 (IBM, Armonk, NY, USA). ImageJ 1.54 was used for band quantification in all blotting experiments and fluorescence intensity and graphs were generated with GraphPad Prism 8.0.1 (GraphPad Software, La Jolla, CA, USA). Significant pathways were enriched via the Kyoto Encyclopedia of Genes and Genomes (KEGG) database, with significance labeled as * $p < 0.05$, ** $p < 0.01$, *** $p < 0.001$.

3. Results

3.1 Lysosome Extraction From Pancreatic Tissues

This study focused on the early stage of AP using a cerulein mouse model. Serum and pancreatic tissues were collected as displayed (Fig. 1A). While biochemical assays demonstrated peak serum amylase (α-AMY) activities at 3 h (Fig. 1B), pathological scoring results of H&E staining confirmed the most evident pathological changes at this time point, including acinar swelling and edema (Fig. 1C). Based on biochemical and histopathological data, TEM-based qualitative ultrastructural assessment, including lysosomal quantification, was scheduled for 3 h after final cerulein injection. At 3 h, cerulein-induced AP model mice displayed increased lysosome levels and size compared with saline controls (Fig. 1D), suggesting that lysosomal potentially mediates AP initiation.

Subsequently, lysosomes were isolated from AP and control pancreatic tissues (Fig. 2A). Sample purity was verified using western blot analysis (Fig. 2B), followed by integrated proteomic/metabolomics analysis.

3.2 Lysosomal Protein Profiles in Pancreatic Tissues of AP Model Mice

Lysosomal proteomic analysis was conducted using high-resolution MS (peptide mass error ±10 ppm) with stringent filtering (peptide false discovery rate ≤0.01; protein false discovery rate ≤0.01), and 54,463 peptides and 6980 proteins were identified (**Supplementary Tables 1–4**; Fig. 3A). Quality control demonstrated tight alignment of median protein expression across biological replicates, with principal component analysis (PCA) confirming high intra-group reproducibility (Fig. 3B,C).

Quantitative analysis revealed 6750 proteins, including 1049 differentially abundant proteins in AP model mice (568 downregulated/481 upregulated; Fig. 3D). The top

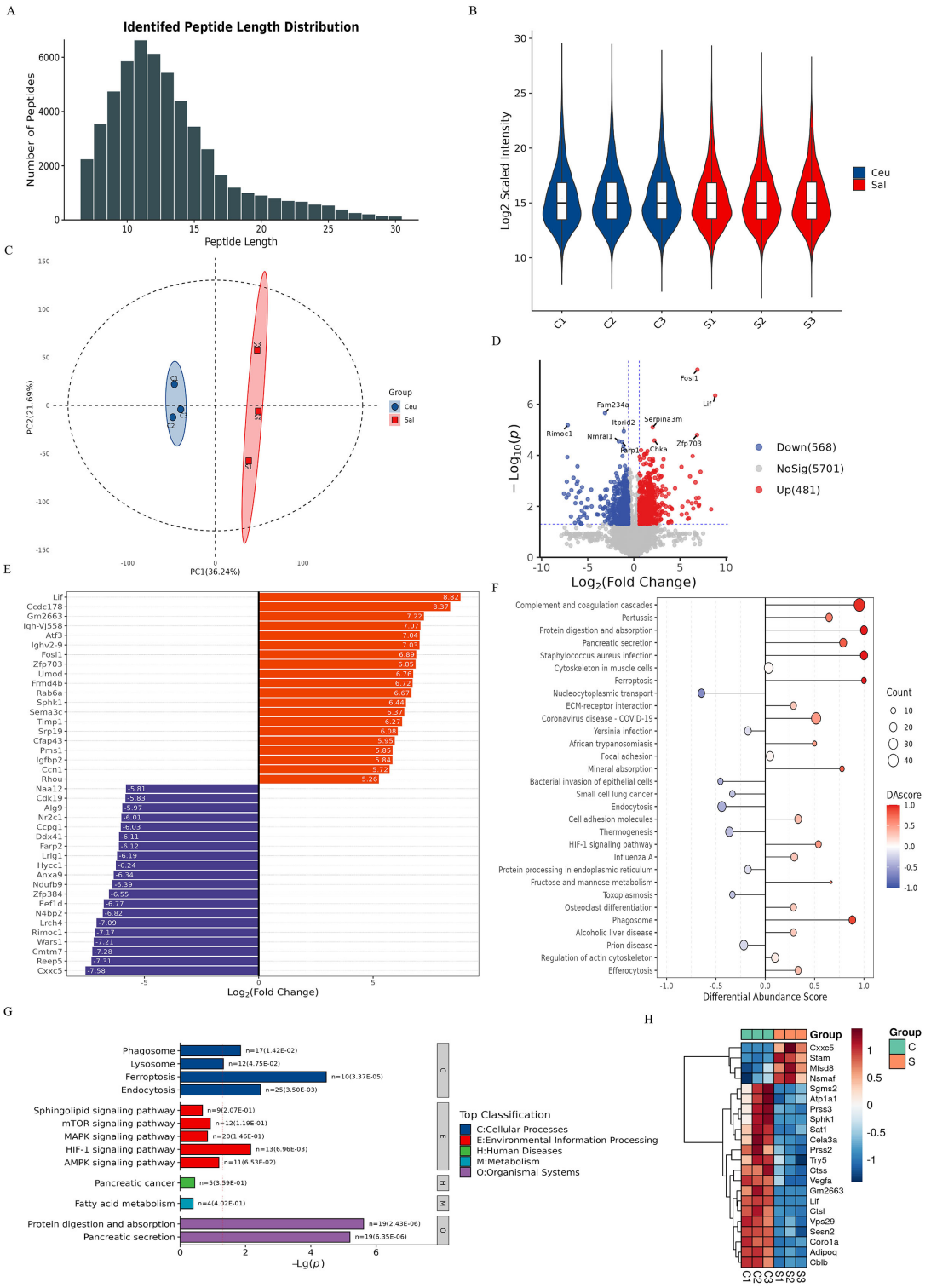


Fig. 3. Proteomics analysis of lysosomes in AP mice (n = 3 per group). (A–C) Sample quality control analysis. (A) Distribution of peptide segment lengths. (B) The violin plot of the intensity of the expression distribution of the samples. (C) Principal component analysis (PCA) plot of indicated samples. (D) The volcano plot of the changes in proteins (blue indicates downregulation, red indicates upregulation, and gray indicates no difference). (E) The difference multiple bar chart of the top 20 proteins in the up-regulation and down-regulation rankings. (F) The top 30 Kyoto Encyclopedia of Genes and Genomes (KEGG) pathways. (G) The top 30 and the pathways of interest. (H) The heat map of the top 22 proteins that have significant changes in the g graph. There were no exclusions in animals.

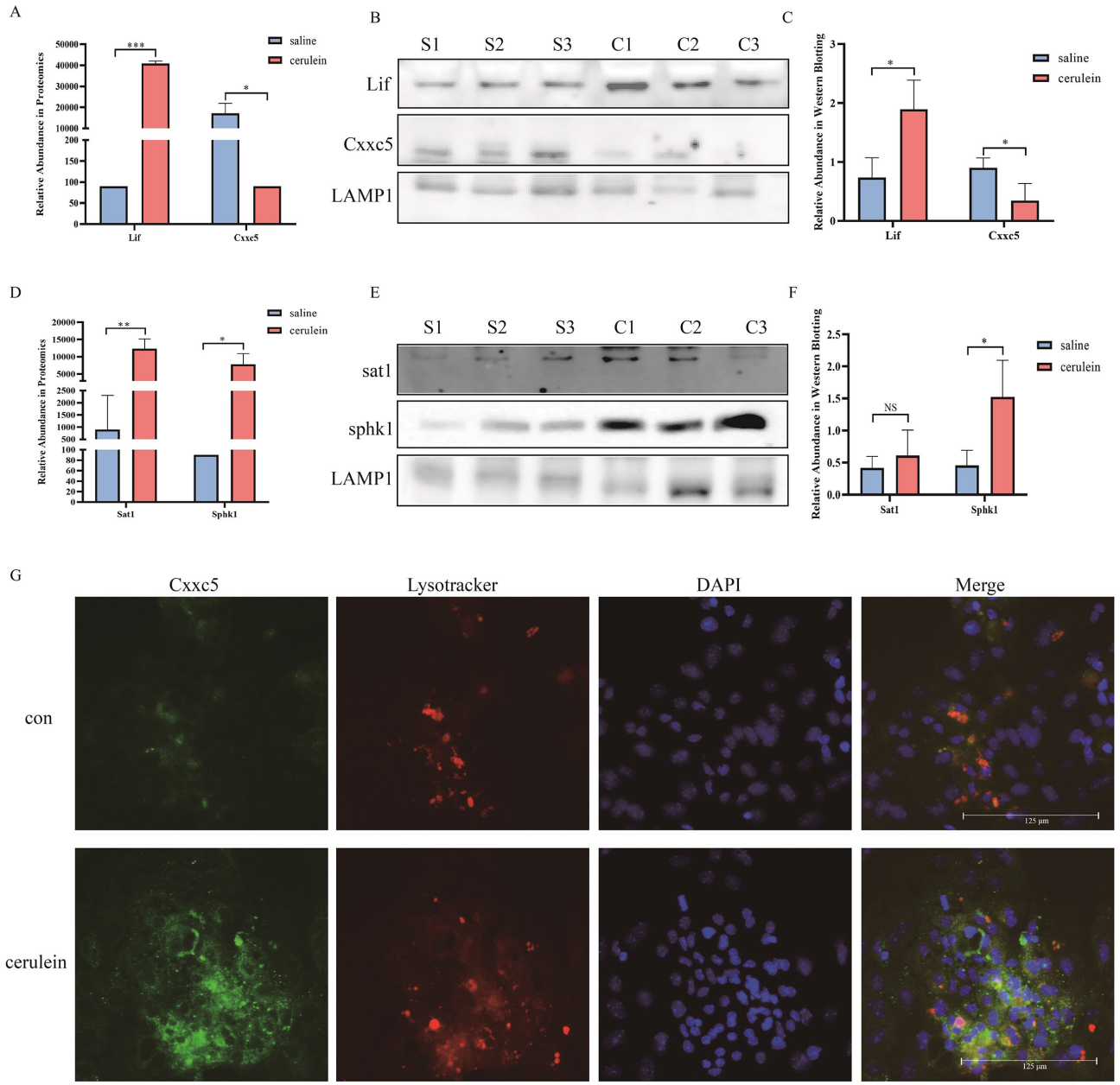


Fig. 4. Validation of proteomics results (n = 3 per group). (A,D) The detection results of Lif, Cxxc5, Sat1 and Sphk1 in proteomics. (B,E) The protein levels of Lif, Cxxc5, Sat1 and Sphk1 in the same lysosome samples were analyzed by western blotting. (C,F) The quantitative results of the indicated proteins, the graph represented as Mean ± SD. (G) Fluorescence co-localization characterization of Cxxc5 protein and Lyso-Tracker Red probe in primary pancreatic acinar cells. Scale bar: 125 μm. Significant differences between the two groups were analyzed using Student's *t*-tests. * $p < 0.05$, ** $p < 0.01$, *** $p < 0.001$. There were no exclusions in animals.

20 upregulated or downregulated proteins were also highlighted, including Leukemia inhibitory factor (Lif), Coiled-coil domain-containing protein 178 (Ccdc178), Predicted gene 2663 (Gm2663), CKLF-like MARVEL transmembrane domain-containing protein 7 (Cmtm7), Receptor accessory protein 5 (Reep5), and Cxxc5 (Fig. 3E). KEGG enrichment (DA scores) identified the top 30 pathways (Fig. 3F). Upregulated pathways included complement and coagulation cascades, pertussis, protein digestion and absorption, pancreatic secretion, *Staphylococcus aureus* infection, the cytoskeleton in muscle cells, and ferroptosis. In contrast, downregulated pathways included nucleocytoplasmic transport, *Yersinia* infection, and bacterial invasion of epithelial cells.

Biologically relevant pathways with substantial changes were prioritized (Fig. 3G). The phagosome, lysosome, ferroptosis, endocytosis, sphingolipid signaling, mTOR/MAPK/HIF-1/AMPK signaling, protein digestion

and absorption, and pancreatic secretion pathways were significantly enriched in lysosomes from AP model mice, indicating tight lysosomal regulation in cerulein-induced AP. The heatmap of the top 22 differentially expressed proteins related pathways were shown in Fig. 3H. Lif and Cxxc5 were the most significantly altered targets (Fig. 3H). Lif, Cxxc5, diamine acetyltransferase 1 (Sat1), and Sphingosine kinase 1 (Sphk1) were selected for western blot validation, and the expression trends of these proteins partially matched the proteomics data (Fig. 4A–F). Consistent with the proteomics results, immunofluorescence showed that the co-localization of Cxxc5 with the lysosome probe Lyso-Tracker Red in primary pancreatic acinar cells was significantly reduced in the cerulein-treated group compared with the control group (Fig. 4G). These findings revealed significant perturbations in the lysosomal pathways involved in ferroptosis, sphingolipid metabolism, signal transduction cascades, and protein synthesis/metabolism during AP progression.

3.3 Lysosomal Metabolomic Alterations in Pancreatic Tissues of AP Model Mice

Untargeted metabolomic profiling of pancreatic tissue–derived lysosomes in AP model mice identified 1450 metabolites across 17 distinct biochemical categories (Fig. 5A and **Supplementary Table 5**). Orthogonal partial least squares-discriminant analysis (OPLS-DA) indicated clear segregation between the cerulein-treated and control cohorts (Fig. 5B,C). Furthermore, the OPLS-DA model identified 438 differentially expressed metabolites, of which 237 were upregulated and 201 were downregulated (**Supplementary Table 5**). The statistical significance of these metabolites was rigorously validated using volcano plot analysis and hierarchical clustering heatmap visualization (Fig. 5D,E).

Based on the variable importance in projection (VIP) values, the top 30 significantly differentially abundant metabolites were identified, including N1-AcSpd, microcystin LF, adrenic acid, and spermidine, all of which exhibited statistically significant VIP values (Fig. 5F). Pearson correlation coefficient analysis of the top 300 differentially abundant metabolites revealed extensive co-regulatory networks, as visualized by circos plots (Fig. 5G). Secondary KEGG pathway enrichment analysis detected 37 significantly enriched pathways, with significant perturbations in cell growth and death, membrane transport, signal transduction, amino acid metabolism, lipid metabolism, global and overview maps, energy metabolism, and digestive system in the cerulein-treated group (Fig. 5H).

Based on metabolomic alterations, N1-AcSpd (the most significantly upregulated) and NAD^+ (not among the top 30 differentially abundant metabolites but significantly downregulated, and a commercial detection kit was available) were chosen as representative metabolites and experimentally validated. Consistent with metabolomics data, the results showed significantly increased N1-AcSpd levels and significantly decreased NAD^+ levels (Fig. 6 and **Supplementary Fig. 2**). Therefore, these findings support systematic remodeling of lysosomal pathways in cerulein-induced AP model mice, including cell growth/death signaling, lipid metabolism, amino acid metabolism, and interconnected signal transduction cascades.

3.4 Integrated Proteomic/Metabolomic Analysis

To overcome the inherent limitations of single-omics approaches, we integrated quantitative proteomic and metabolomic datasets, thereby characterizing concomitant dysregulation of signaling pathways in cerulein-induced AP models. Pearson correlation analysis of differentially altered metabolites and proteins revealed significant associations involving 30 metabolites: tetrahydropyridine, sebuthylazine, 7,2'-dihydroxy-4',5'-methylenedioxyisoflavan-4-ol, microcystin-LF, Ile-Gly-Phe, nitrile-heptanoic acid, spermidine, 1-acetyl-15,16-dimethoxy-aspidospermidine-17,21-diol, pseudouridine-5'-phosphate, scabioside C, nortricycloekasantalic acid, actinioerythrol, indol-3-yl pyruvic acid, 6-methoxy-4-methylcoumarin, N1-AcSpd, 1-methyl-2-pyrrolidinone, 3-hydro xysebacic acid, clathrin A, myristic acid, α-hydroxyglutaric acid, maltotetraose, PE(18:1(9Z)/0:0), isopimpinellin, pityiacitrin, CMP, PFAP-diPAP, adrenic acid, Leu-Ala-Asp, desmarestene, and AGN-PC-0LP8QO. These metabolites exhibited numerous significant correlations with dysregulated proteins: Carboxypeptidase N catalytic chain (Cpn1), Coagulation factor XIII B chain (F13b), Calcipressin-1 (Rcan1), Immunoglobulin heavy variable 1-50 (Ighv1-50), Prothrombin (F2), Inter-alpha-trypsin inhibitor heavy chain H2 (Itih2), Carboxylesterase 1C (Ces1c), Mannose-binding protein C (Mbl2), Angiotensinogen (Agt), Transthyretin (Ttr), Geranylgeranyl pyrophosphate synthase (Ggps1), Neutrophil cytosol factor 2 (Ncf2), Phospholipase B-like 1 (Plbd1), Sestrin-2 (Sesn2), Vacuolar protein sorting-associated protein 29 (Vps29), Rho-related GTP-binding protein RhoC (Rhoc), Maleylacetoacetate isomerase (Gstz1), Immunoglobulin heavy variable 15-103 (Igkv15-103), Fibulin-2 (Fbln2), Adiponectin (Adipoq), Receptor-type tyrosine-protein phosphatase kappa (Ptprk), Constitutive coactivator of PPAR-gamma-like protein 2 (Fam120c), Receptor-type tyrosine-protein phosphatase F (Ptprf), Homer protein homolog 2 (Homer2), Upstream-binding protein 1 (Ubp1), Extracellular superoxide dismutase [Cu-Zn] (Sod3), Peptidyl-prolyl cis-trans isomerase FKBP8 (Fkbp8), Lipoma-preferred partner homolog (Lpp), Myosin XVB (Myo15b), and Epithelial discoidin domain-containing receptor 1 (Ddr1) (Fig. 7A). These interactions suggest that lysosomal metabolite–protein networks may play critical regulatory roles in cerulein-induced AP progression.

Integrated KEGG pathway analysis of proteomic and metabolomic datasets yielded 109 overlapping pathways

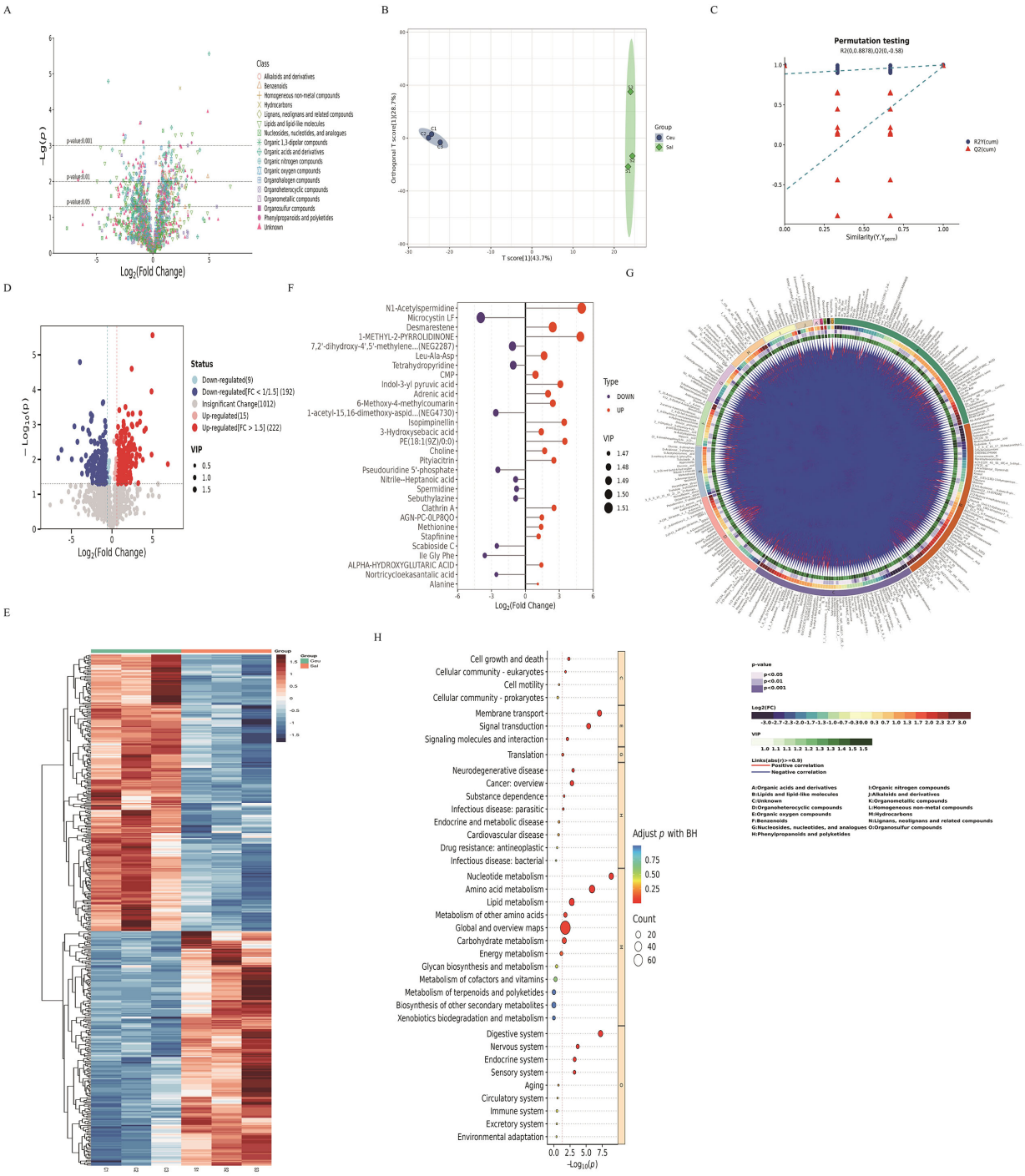


Fig. 5. Metabolomics analysis of lysosomes in AP mice (n = 3 per group). (A) Volcano Plot, metabolites were classified using Human Metabolome Database (HMDB) Superclass, and different colors and shapes were used to represent them on the graph. (B) OPLS-DA score scatter plot of the samples. (C) Permutation validation plot of the orthogonal partial least squares discriminant analysis model (OPLS-DA). (D) The volcano graph of the changes in metabolites (blue indicates a decrease, red indicates an increase, and gray indicates no difference). (E) Heatmap of the hierarchical clustering results of the differential metabolites. (F) Based on the variable weights obtained from the OPLS-DA model, the top 30 differentially expressed metabolites with significant differences were identified. The larger the point, the greater the VIP value. Red points indicate upregulation, and blue points indicate downregulation (**Supplementary Table 5**). (G) The Circos circular graph of the direct relationships among the top 300 metabolites. (H) Bubble chart of the second layer KEGG pathway enrichment of the differential metabolites resulted in the top 37 pathways. The size of the bubbles represents the quantity of the metabolites. There were no exclusions in animals.

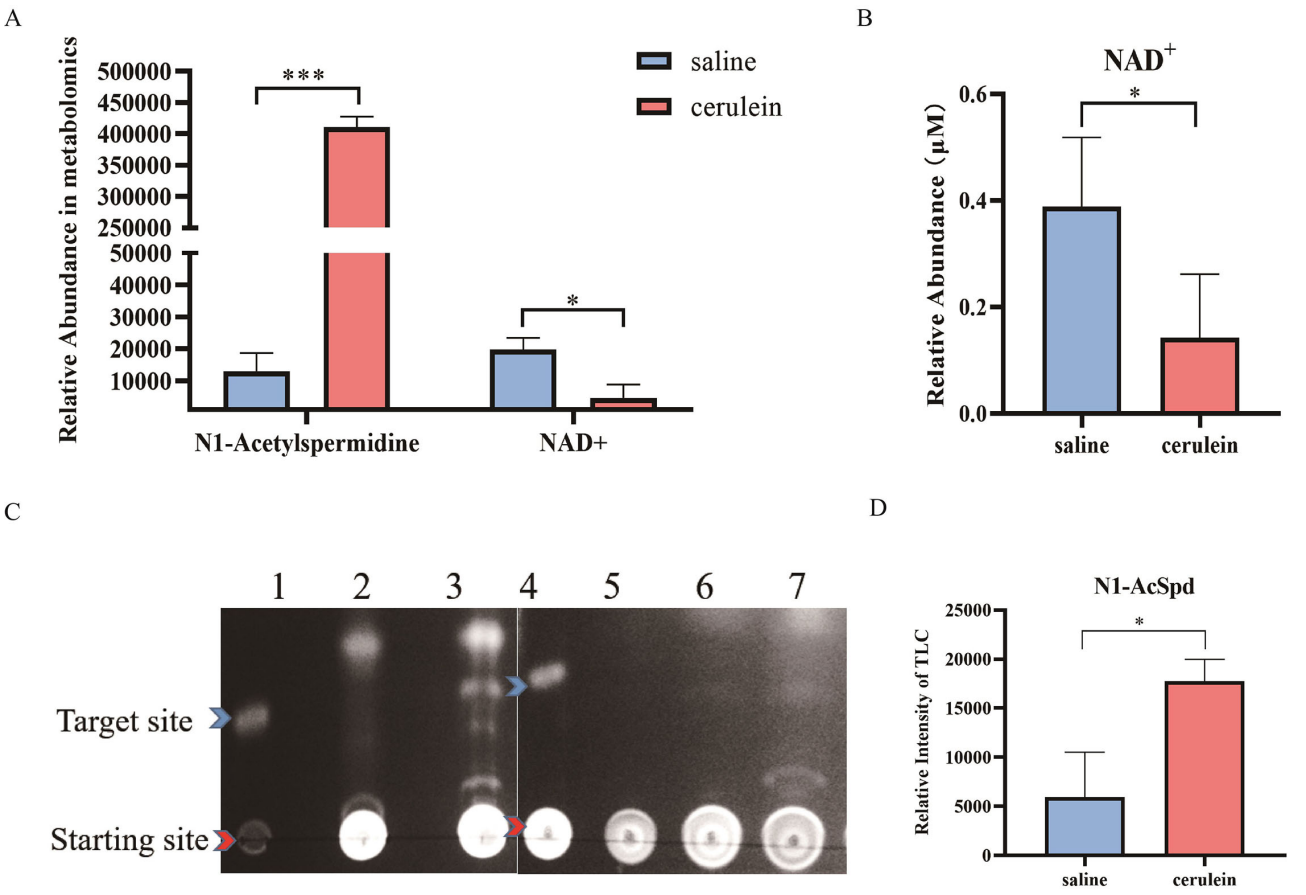


Fig. 6. Validation of metabolomics results. (A) Detection results of N1-AcSpd and NAD^+ in metabolomics (n = 3 per group). (B) The kit was used to measure the content of NAD^+ in lysosomes (n = 5 in saline group, n = 3 in cerulein group). (C,D) Thin-layer chromatography method was used to determine N1-AcSpd. Lanes 1 and 4: 100 μM N1-AcSpd standard, volume 2.5 μL; Lanes 2 and 5: saline group, volume 7.5 μL; Lanes 3, 6, and 7: cerulein group, volume 7.5 μL, and (D) represents the quantitative result of (C). Significant differences between the two groups were analyzed using Student's *t*-tests. * $p < 0.05$, *** $p < 0.001$. There were no exclusions in animals.

underlying the pathogenesis of AP (Fig. 7B). Hierarchical clustering heatmap visualization indicated 39 shared pathways that exhibited significant alterations in both proteomic and metabolomic profiles (Fig. 7C). Among the top 25 dysregulated pathways were biosynthesis amino acid (metabolic regulation), HIF-1 signaling (signal transduction), lysosome (transport and catabolism), ferroptosis (cell fate determination), and protein digestion and absorption (nutrient processing) (Fig. 7D).

Integrated KEGG mapping indicated significant sphingolipid–ferroptosis crosstalk (Fig. 7E). Experimental validation confirmed sphingolipid metabolic rewiring, characterized by significant upregulation of Sphk1 protein expression. Concurrently, we reconstructed the polyamine metabolic regulatory network from the differentially abundant proteins and metabolites (Fig. 7F), thereby elucidating coordinated lysosomal stress responses during AP progression.

3.5 N1-Acetylspermidine-Induced Pancreatic Injury

The metabolite N1-AcSpd, which exhibited the most pronounced variation in concentration, was intraperitoneally administered to mice at gradient doses (0/5/10 mg/kg) (Fig. 8A). Serum amylase activity assays and pancreatic H&E staining indicated that administration of a 10-mg/kg dose robustly induced AP hallmarks (Fig. 8B,C). Hence, 10 mg/kg N1-AcSpd was selected for mechanistic investigation. Considering the pivotal roles of lysosome-mediated autophagy and apoptosis in AP pathology [7], autophagy (LC3B) and apoptosis (Bcl2/Bax) markers were subjected to western blot analysis. No significant changes were detected compared with the controls (Fig. 8D–F), indicating that N1-AcSpd may drive pathogenesis via non-canonical pathways.

Integrated KEGG pathway analysis identified a significant correlation between Sat1 and ferroptosis (Fig. 7E), with Sat1 catalyzing spermidine to form N1-AcSpd (Fig. 7F). Under N1-AcSpd treatment, western blotting showed a significant decrease in the protein level of the ferropto-

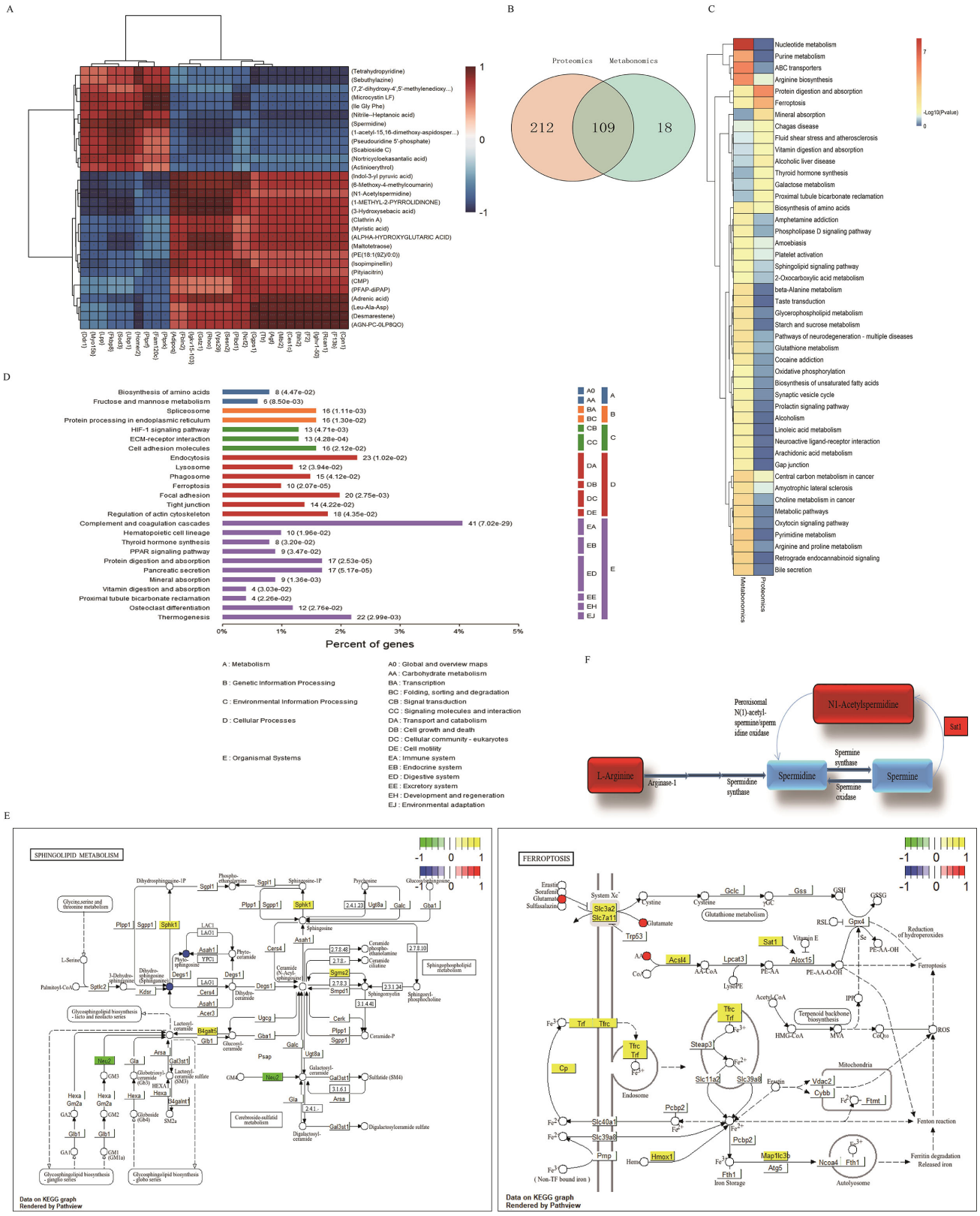


Fig. 7. Integrated Analysis of Proteomics and Metabolomics (n = 3 per group). (A) The correlation-based hierarchical clustering heatmap of the top 30 metabolites and proteins ranked by the absolute values of their correlation coefficients. (B) Venn diagram of the 109 shared KEGG pathways between the two omics datasets. (C) Heatmap of the distribution of pathways with significant differences in metabolomics and proteomics. (D) Conjoint analysis enriched the top 25 KEGG pathways. (E) KEGG pathway diagrams, respectively representing, sphingolipid signaling pathway and ferroptosis. (F) The polyamine metabolic pathway map was generated based on DEFs and metabolites, where red indicates upregulation and blue indicates downregulation. There were no exclusions in animals.

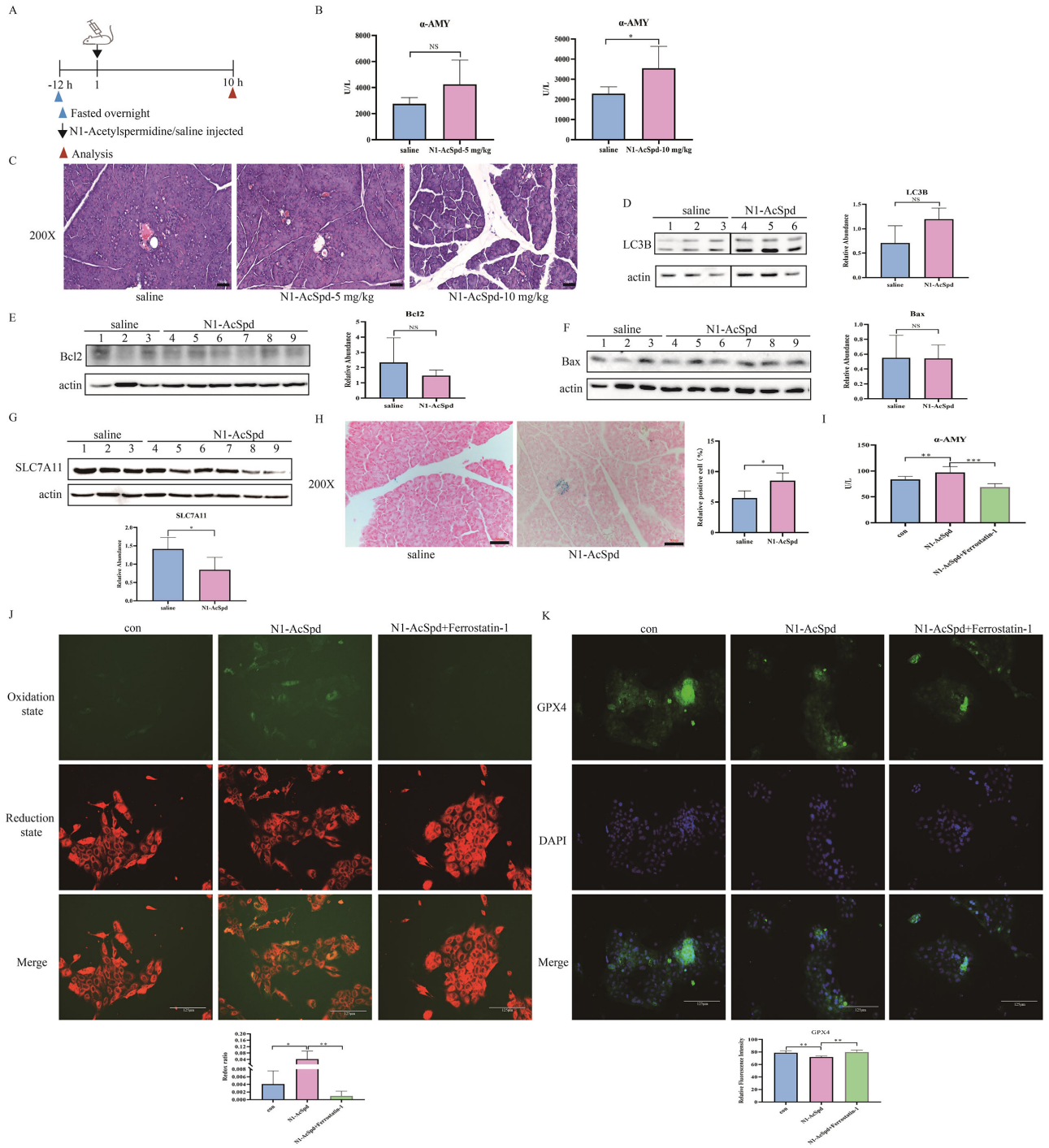


Fig. 8. N1-AcSpd induced pancreas injury in mice. (A) Schematic diagram of mouse model establishment by intraperitoneal injection of N1-AcSpd. (B,C) The biochemical analysis of amylase and the H&E staining of pancreatic tissue (n = 3 in saline group, n = 5 in 5 mg/kg group; n = 5 in saline group, n = 4 in 10 mg/kg group). Scale bar: 50 μm. (D–G) Indicated proteins in pancreas under the indicated treatment (N1-AcSpd, 10 mg/kg) were analyzed by western blotting, and protein intensity was qualified and visualized as the graph with mean ± SD. (H) Prussian blue staining of the pancreas tissues (n = 3 in saline group, n = 4 in 10 mg/kg group). Scale bar: 50 μm. (I) Amylase levels in the medium from primary pancreatic acinar cells were measured using an automatic biochemical analyzer (n = 7 per group). (J,K) The fluorescence imaging and quantitative analysis results of lipid peroxidation andGPX4 in primary pancreatic acinar cells under different treatment conditions (n = 5 per group). Scale bar: 125 μm. Significant differences between the two groups were analyzed using Student's *t*-tests. Significant differences among more than two groups were analyzed using ANOVA. NS, not significant, * $p < 0.05$, ** $p < 0.01$, *** $p < 0.001$. GPX4, glutathione peroxidase 4. There were no exclusions in animals.

sis regulator SLC7A11 (xCT subunit) compared with the controls (Fig. 8G), while Prussian blue staining confirmed increased iron deposition (Fig. 8H). To further elucidate the regulatory role of N1-AcSpd in pancreatic acinar cells, primary mouse pancreatic acinar cells were isolated for *in vitro* culture. After indicated pretreatment, it was revealed that, compared with the blank control group, treatment with 100 μM N1-AcSpd significantly increased secretory amylase levels, markedly enhanced lipid peroxidation and decreased glutathione peroxidase 4 (GPX4) (Fig. 8I–K). Nevertheless, the ferroptosis inhibitor Ferrostatin-1 reversed the N1-AcSpd-induced increase in amylase levels and lipid peroxidation, and decrease in GPX4 (Fig. 8I–K). These findings indicate that N1-AcSpd induces pancreatic injury through ferroptosis.

4. Discussion

Cerulein disrupts lysosome–zymogen granule compartmentalization in pancreatic acinar cells, prompting abnormal contact between lysosomal hydrolases (e.g., cathepsin B) and trypsinogen. This interaction culminates in premature pancreatic enzyme activation in AP [23]. In the cerulein-induced AP model mice in this study, an integrated proteomic/metabolomic analysis of pancreatic lysosomes identified 1049 differentially abundant proteins (568 downregulated and 481 upregulated) and 438 differentially abundant metabolites (237 upregulated and 201 downregulated), concurrent with significant alterations in lysosomal biological functions. Key molecular changes were experimentally validated, notably revealing that N1-AcSpd induced pancreatic injury through ferroptosis. This study represents the first multi-omics characterization of lysosomal roles in AP pathogenesis through metabolic reprogramming, signal transduction modulation, and cell death regulation.

Molecular mechanisms underlying AP have been investigated using proteomic analysis, revealing multiple biomarkers associated with pancreatic disease [24]. In this study, high-resolution MS-based proteomics was used to comprehensively map the lysosomal proteome in cerulein-induced AP, resulting in the construction of the first protein interaction network during AP progression. KEGG enrichment analysis of 1049 differentially abundant proteins delineated three core pathological modules: (1) digestive enzyme hyperactivation and membrane transport imbalance, (2) ferroptosis activation and metabolic reprogramming, and (3) cellular stress and quality control dysregulation. Protein interaction analysis mapped these perturbations to critical pathways: protein digestion and absorption (ko04974), pancreatic secretion (ko04972), HIF-1 signaling pathway (ko04066), lysosome (ko04142), phagosome (ko04145), ferroptosis (ko04216), and sphingolipid signaling pathway (ko04071). These findings highlight that combined targeting of premature zymogen activation, ferroptosis signaling, and sphingolipid dysregulation may represent a novel therapeutic strategy.

In addition, our proteomic analysis revealed significant upregulation of a large panel of immunoglobulin (Ig) proteins. As is well established, aberrant elevation of the IgG4 subclass represents a definitive hallmark of type 1 autoimmune acute pancreatitis: extensive infiltration of IgG4-positive plasma cells into the pancreatic parenchyma triggers lymphoplasmacytic sclerosing inflammation, which directly drives hallmark acute clinical manifestations including pancreatic swelling and biliary stricture [25]. Previous mechanistic studies have demonstrated that circulating IgG is internalized by endothelial cells via pinocytosis; within the acidic endosomal microenvironment, IgG molecules that fail to bind to the neonatal Fc receptor (FcRn) evade recycling and are ultimately shuttled directly into lysosomes for hydrolytic degradation, a pathway widely recognized as the core mechanism maintaining IgG homeostasis in peripheral blood [26]. Since these immunoglobulin-related pathways are not the central focus of the present study, we did not investigate their roles.

In our proteomic analysis, data regarding digestive KEGG pathways and the Na^+/K^+-ATPase α1 subunit (Atp1a1), with alteration in case of AP, were reported to be associated with lysosomal function [27]. Specifically, the digestive enzyme Cela3a exhibited pronounced upregulation in our study, although its role in AP remains unknown. Notably, ferroptosis has been associated with pancreatic injury [28,29,30], and our data revealed that, within the ferroptosis signaling pathway, transferrin system components (Trf and Tfrc), SLC7A11, and Sat1 were upregulated.

Our proteomic findings showed that dysregulation of neutral sphingomyelinaseactivation associated factor (Nsmaf) and Sphk1 was particularly pronounced within the sphingolipid signaling pathway. Nsmaf modulates neutral sphingomyelinase activity and lysosomal morphology via the scaffold protein Receptor for Activated Protein C Kinase 1 (RACK1) [31]. Sphk1 has been shown to contribute to malignancy associated with chronic pancreatitis [32] and has recently been found to regulate lysosomal enzyme activity via S1P receptor–independent mechanisms [33]. These converging pathways suggest that sphingolipid signaling may serve as a regulator of lysosomal function in AP.

This study represents the first application of non-targeted metabolomics to analyzing metabolic perturbations in the lysosomal compartment of pancreatic tissues from AP model mice. Critical metabolic classes include polyamines, lipids, sphingolipids, ferroptosis-associated metabolites, peptides, amino acids, and nucleotides. Taken together, these findings comprehensively map early metabolic rewiring events in AP lysosomes.

It is well established that polyamine metabolism is associated with AP pathogenesis. Prior research suggests that severe depletion of high-concentration polyamines in pancreatic tissue correlates with the progression of injury [34]. Activated polyamine catabolism constitutes a conserved

pathway in AP initiation, in which polyamine analogs inhibit trypsinogen activation and mitigate AP symptoms in Sat1-transgenic mouse models [35]. In these Sat1-transgenic models, N1-AcSpd was found to be present. Previous reports have suggested that Sat1 upregulation induces AP symptoms owing to decreased polyamine levels. Consistently, our analysis demonstrated significant reductions in spermine and spermidine levels, accompanied by a marked increase in N1-AcSpd in AP groups. These findings imply that upregulated Sat1 activity may convert spermidine into N1-AcSpd during cerulein challenge. Although the existing literature has tended to focus on Sat1 transgenic rodents, we prioritized the functional investigation of N1-AcSpd based on the most significant alteration.

Exogenous administration of N1-AcSpd yielded robust AP pathological hallmarks in mice. Integrated proteomic and metabolomic profiling implicated ferroptosis pathway activation in N1-AcSpd-driven pancreatic injury, as validated by western blot analysis and Prussian blue staining. Notably, it has recently been reported that fraxinellone (FRA) induces ferroptosis in hypertrophic scar fibroblasts through GPX4 suppression. Notably, during FRA-induced ferroptosis, cathepsin B (CTSB) was released, contributing to Sat1-mediated lipid peroxidation [36]. However, our data showed a reduction in total CTSB expression under N1-AcSpd treatment (data not shown). It remains to be further investigated whether the translocation of CTSB contributes to ferroptosis.

Based on the results of integrated multi-omics analysis, we identified and chose the pathways mainly involved in the biosynthesis of amino acids (metabolic regulation), the HIF-1 signaling pathway (signal transduction), the lysosome (transport and catabolism), ferroptosis (cell fate), and protein digestion and absorption (nutrient uptake) (Fig. 7D). Existing research has confirmed that the abnormal activation of amino acid metabolism pathways in pancreatic tissue under circadian disruption can significantly increase the risk of pancreatitis [37]. The HIF-1 signaling pathway is directly involved in the pathological injury process of AP via multiple mechanisms, including downstream pro-inflammatory factor release, oxidative stress cascade amplification, and ferroptosis induction [38,39,40]. There have been reports that the level of protein catabolism at this stage can increase by 80% compared with the baseline, and overall energy consumption can increase by 20%, indicating that the body's demand for nutrient substrates is significantly upregulated under AP conditions [41]. The synergistic enrichment results also emphasize that metabolic reprogramming, hypoxia signal disorder, abnormal cell death, and nutrient metabolism imbalance are the core pathological features for AP initiation with potential research value.

The core early pathophysiology of AP encompasses three key links: abnormal zymogen activation, calcium dyshomeostasis, and autophagy dysfunction. Premature trypsin activation serves as a very early landmark event. Pathological insults trigger cytoplasmic calcium overload via endoplasmic reticulum and mitochondrial dysfunction, which, combined with autophagic flux blockade caused by impaired autophagosome–lysosome fusion, leads to acinar cell injury and necrosis [42]. Non-surgical regimens centered on organ protection are the predominant strategies for treating early-phase AP. Furthermore, active monomers, compound preparations, and external therapies involving traditional Chinese medicine have demonstrated definite adjuvant value. Notably, cutting-edge technologies such as those utilizing nanotechnology and extracellular vesicles provide new dimensions for AP precision therapy. Targeting lysosomal structural disruption represents a highly promising mechanism-specific intervention strategy [42,43], underscoring the importance of multi-omics lysosome analysis in AP.

5. Limitations

The following limitations of this study should be noted. First, extensive pathway enrichment analyses were performed, but only a subset was discussed, potentially overlooking other important pathways. We intend to conduct further in-depth research on several representative pathways mentioned in the discussion section. Second, when conducting the integrated metabolomics/proteomics analysis, other potential metabolites may not have considered. Third, the sample size was relatively small, and no clinical samples were included for verification. Fourth, given the lack of multi-omics analyses of the temporal and spatial progression of lysosomes in AP model mice, carefully designed future studies that address this gap may be expected to provide a deeper understanding of the changing characteristics of lysosomes during the occurrence and development of AP.

6. Conclusion

This study revealed, for the first time, significant upregulation of ferroptosis pathway proteins, and marked fluctuations in polyamine metabolites in AP pancreatic lysosomes. Notably, Sphk1-related pathways may play a role in AP progression. The study also innovatively established a relationship between exogenous N1-AcSpd injection and ferroptosis pathways in an AP model.

Availability of Data and Materials

The mass spectrometry proteomics data have been deposited in the ProteomeXchange Consortium (https://proteomecentral.proteomexchange.org) via the iProX partner repository with the dataset identifier PXD071419. The datasets used and analyzed during the current study are available from the corresponding author on reasonable request.

Author Contributions

WL: formal analysis, investigation, visualization, writing – original draft; JC: formal analysis, investigation, visualization, writing – original draft; TS: animal study, writing; JX: conceptualization, funding acquisition, project administration, supervision, writing – original draft, writing – review & editing. All authors have participated sufficiently in the work and agreed to be accountable for all aspects of the work. All authors contributed to editorial changes in the manuscript. All authors read and approved the final manuscript.

Ethics Approval and Consent to Participate

All animal care and experimental procedures were approved by the Animal Ethics Committee of Guilin Medical University (Approval No. GLMC-IACUC-20251060) and conducted in accordance with the ARRIVE guidelines and the national standard GB/T 35892-2018 for laboratory animal welfare.

Acknowledgment

We thank LetPub for its linguistic assistance during the preparation of this manuscript.

Funding

This study was supported in part by the National Natural Science Foundation of China (No. 82460136), Natural Science Foundation of Guangxi Province (No. 2025GXNSFAA069836) and Guangxi Bagui Program for Young Talents.

Conflicts of Interest

The authors declare no conflicts of interest.

Supplementary Material

Supplementary material associated with this article can be found, in the online version, at https://doi.org/10.31083/FBL56885.

References

[1] Zhou R, Wu Q, Yang Z, Cai Y, Wang D, Wu D. The Role of the Gut Microbiome in the Development of Acute Pancreatitis. International Journal of Molecular Sciences. 2024; 25: 1159. https://doi.org/10.3390/ijms25021159

[2] Zhang R, Ling X, Guo X, Ding Z. MGST1 Protects Pancreatic Ductal Cells from Inflammatory Damage in Acute Pancreatitis by Inhibiting Ferroptosis: Bioinformatics Analysis with Experimental Validation. International Journal of Molecular Sciences. 2025; 26: 1899. https://doi.org/10.3390/ijms26051899

[3] Beij A, Verdonk RC, van Santvoort HC, de-Madaria E, Voermans RP. Acute Pancreatitis: An Update of Evidence-Based Management and Recent Trends in Treatment Strategies. United European Gastroenterology Journal. 2025; 13: 97–106. https://doi.org/10.1002/ueg2.12743

[4] Chen XQ, Yang Q, Chen WM, Chen ZW, Guo GH, Zhang X, et al. Dual role of lysosome in cancer development and progression. Frontiers in Bioscience (Landmark Edition). 2024; 29: 393. https://doi.org/10.31083/j.fbl2911393

[5] Wu Y, Wang H, Xu H. Autophagy-lysosome pathway in insulin & glucagon homeostasis. Frontiers in Endocrinology. 2025; 16: 1541794. https://doi.org/10.3389/fendo.2025.1541794

[6] Zierke L, John D, Gischke M, Tran QT, Sendler M, Weiss FU, et al. Initiation of acute pancreatitis in mice is independent of fusion between lysosomes and zymogen granules. Cellular and Molecular Life Sciences: CMLS. 2024; 81: 207. https://doi.org/10.1007/s00018-024-05247-7

[7] Mareninova OA, Sendler M, Malla SR, Yakubov I, French SW, Tokhtaeva E, et al. Lysosome associated membrane proteins maintain pancreatic acinar cell homeostasis: LAMP-2 deficient mice develop pancreatitis. Cellular and Molecular Gastroenterology and Hepatology. 2015; 1: 678–694. https://doi.org/10.1016/j.jcmgh.2015.07.006

[8] Hao M, Sebag SC, Qian Q, Yang L. Lysosomal physiology and pancreatic lysosomal stress in diabetes mellitus. EGastroenterology. 2024; 2: e100096. https://doi.org/10.1136/egastro-2024-100096

[9] Zhang H, Zhou Y, Yu B, Deng Y, Wang Y, Fang S, et al. Multi-Omics Approaches to Discover Biomarkers of Thyroid Eye Disease: A Systematic Review. International Journal of Biological Sciences. 2024; 20: 6038–6055. https://doi.org/10.7150/ijbs.103977

[10] Su F, Su M, Wei W, Wu J, Chen L, Sun X, et al. Integrating multi-omics data to reveal the host-microbiota interactome in inflammatory bowel disease. Gut Microbes. 2025; 17: 2476570. https://doi.org/10.1080/19490976.2025.2476570

[11] Liu X, Peng T, Xu M, Lin S, Hu B, Chu T, et al. Spatial multi-omics: deciphering technological landscape of integration of multi-omics and its applications. Journal of Hematology & Oncology. 2024; 17: 72. https://doi.org/10.1186/s13045-024-01596-9

[12] Wang J, Hu Y, Zhao K, Fan J, Zhu J, Li Q, et al. Comprehensive analysis of the expression of cell adhesion molecules genes in hepatocellular carcinoma and their prognosis, and biological significance. Frontiers in Bioscience (Landmark Edition). 2024; 29: 76. https://doi.org/10.31083/j.fbl2902076

[13] Wang R, Wang Y, Tao Y, Hu L, Qiu Q, Pu Q, et al. Temporal Proteomic and Lipidomic Profiles of Cerulein-Induced Acute Pancreatitis Reveal Novel Insights for Metabolic Alterations in the Disease Pathogenesis. ACS Omega. 2023; 8: 12310–12326. https://doi.org/10.1021/acsomega.3c00019

[14] Sun L, Li H, Zhang H, Guo Y, Wang C, Chen S. Proteomics and phosphoproteomics analysis of acute pancreatitis alleviated by forsythoside B. Journal of Proteomics. 2025; 315: 105414. https://doi.org/10.1016/j.jprot.2025.105414

[15] Xu H, Zhang L, Kang H, Zhang J, Liu J, Liu S. Serum Metabonomics of Mild Acute Pancreatitis. Journal of Clinical Laboratory Analysis. 2016; 30: 990–998. https://doi.org/10.1002/jcla.21969

[16] Yang J, Shi N, Wang S, Wang M, Huang Y, Wang Y, et al. Multi-dimensional metabolomic profiling reveals dysregulated ornithine metabolism hallmarks associated with a severe acute pancreatitis phenotype. Translational Research. 2024; 263: 28–44. https://doi.org/10.1016/j.trsl.2023.08.003

[17] Pan F, Wang L, He X, Rong C, Hu Y. Integrative proteomics and metabolomics analysis of the mechanism of pancreatic β-cell dysfunction in aged mice. Frontiers in Endocrinology. 2026; 16: 1723927. https://doi.org/10.3389/fendo.2025.1723927

[18] Li H, Xu Y, Zhou X, Jin T, Wang Z, Sun Y, et al. DIA-Based Proteomic Analysis of Plasma Protein Profiles in Patients with Severe Acute Pancreatitis. Molecules (Basel, Switzerland). 2022; 27: 3880. https://doi.org/10.3390/molecules27123880

[19] Lv T, Zhang C, Zeng Y, Hu L, Huang G, Wang C, et al. Berberine alleviates lipopolysaccharide-induced acute lung injury by

modulating the AMPK-HMGB1-NF-κB signaling axis. Frontiers in Bioscience-Landmark. 2026; 31: 45524. https://doi.org/10.31083/FBL45524

[20] Wildi S, Kleeff J, Mayerle J, Zimmermann A, Böttinger EP, Wakefield L, et al. Suppression of transforming growth factor beta signalling aborts caerulein induced pancreatitis and eliminates restricted stimulation at high caerulein concentrations. Gut. 2007; 56: 685–692. https://doi.org/10.1136/gut.2006.105833

[21] Yao JST, Ladner Y, Amin N'C, Perrin C. Salting-out assisted liquid-liquid extraction (SALLE): Principle, optimization, and applications in blood sample analysis. Journal of Pharmaceutical and Biomedical Analysis. 2025; 257: 116720. https://doi.org/10.1016/j.jpba.2025.116720

[22] Aboul-Enein HY, al-Duraibi IA. Separation of several free polyamines and their acetylated derivatives by ion-pair reversed-phase high performance liquid chromatography. Biomedical Chromatography: BMC. 1998; 12: 291–293. https://doi.org/10.1002/(SICI)1099-0801(199809/10)12:5%3C291::AID-BMC749%3E3.0.CO;2-4

[23] Saluja A, Dudeja V, Dawra R, Sah RP. Early Intra-Acinar Events in Pathogenesis of Pancreatitis. Gastroenterology. 2019; 156: 1979–1993. https://doi.org/10.1053/j.gastro.2019.01.268

[24] Ge P, Luo Y, Zhang G, Chen H. The role of proteomics in acute pancreatitis: new and old knowledge. Expert Review of Proteomics. 2024; 21: 115–123. https://doi.org/10.1080/14789450.2024.2320810

[25] Vemulapalli V, Natha C, Shirwaikar Thomas A. Autoimmune Pancreatitis: A Review. Journal of Clinical Medicine. 2025; 14: 3076. https://doi.org/10.3390/jcm14093076

[26] Andersen JT, Sandlie I. The versatile MHC class I-related FcRn protects IgG and albumin from degradation: implications for development of new diagnostics and therapeutics. Drug Metabolism and Pharmacokinetics. 2009; 24: 318–332. https://doi.org/10.2133/dmpk.24.318

[27] Liu D, Liu M, Lv D, Li Y, Guo H, Lu B, et al. LAPTM4B Confers Resistance to EGFR-TKIs by Suppressing the Proteasomal Degradation of ATP1A1 in Non-small Cell Lung Cancer. International Journal of Biological Sciences. 2026; 22: 1–24. https://doi.org/10.7150/ijbs.115365

[28] Li H, Lin Y, Zhang L, Zhao J, Li P. Ferroptosis and its emerging roles in acute pancreatitis. Chinese Medical Journal. 2022; 135: 2026–2034. https://doi.org/10.1097/CM9.0000000000002096

[29] Ma D, Li C, Jiang P, Jiang Y, Wang J, Zhang D. Inhibition of Ferroptosis Attenuates Acute Kidney Injury in Rats with Severe Acute Pancreatitis. Digestive Diseases and Sciences. 2021; 66: 483–492. https://doi.org/10.1007/s10620-020-06225-2

[30] Liu Q, Wu J, Zhang X, Wu X, Zhao Y, Ren J. Iron homeostasis and disorders revisited in the sepsis. Free Radical Biology & Medicine. 2021; 165: 1–13. https://doi.org/10.1016/j.freeradbiomed.2021.01.025

[31] Möhlig H, Mathieu S, Thon L, Frederiksen MC, Ward DM, Kaplan J, et al. The WD repeat protein FAN regulates lysosome size independent from abnormal downregulation/membrane recruitment of protein kinase C. Experimental Cell Research. 2007; 313: 2703–2718. https://doi.org/10.1016/j.yexcr.2007.04.020

[32] Ketavarapu V, Ravikanth V, Sasikala M, Rao GV, Devi CV, Sripadi P, et al. Integration of metabolites from meta-analysis with transcriptome reveals enhanced SPHK1 in PDAC with a background of pancreatitis. BMC Cancer. 2022; 22: 792. https://doi.org/10.1186/s12885-022-09816-6

[33] Morishige JI, Yoshioka K, Nakata H, Ishimaru K, Nagata N, Tanaka T, et al. Sphingosine kinase 1 is involved in triglyceride breakdown by maintaining lysosomal integrity in brown adipocytes. Journal of Lipid Research. 2023; 64: 100450. https://doi.org/10.1016/j.jlr.2023.100450

[34] Jänne J, Alhonen L, Pietilä M, Keinänen TA, Uimari A, Hyvönen MT, et al. Genetic manipulation of polyamine catabolism in rodents. Journal of Biochemistry. 2006; 139: 155–160. https://doi.org/10.1093/jb/mvj035

[35] Hyvönen MT, Herzig KH, Sinervirta R, Albrecht E, Nordback I, Sand J, et al. activated polyamine catabolism in acute pancreatitis: alpha-methylated polyamine analogues prevent trypsinogen activation and pancreatitis-associated mortality. The American Journal of Pathology. 2006; 168: 115–122. https://doi.org/10.2353/ajpath.2006.050518

[36] Xu W, Lv H, Xue Y, Shi X, Fu S, Li X, et al. Fraxinellone-mediated targeting of cathepsin B leakage from lysosomes induces ferroptosis in fibroblasts to inhibit hypertrophic scar formation. Biology Direct. 2025; 20: 17. https://doi.org/10.1186/s13062-025-00610-5

[37] Li H, Zhang X, He Z, Tong W, Liu W, Ma S, et al. Disruption of the Circadian Rhythm Induces Acute Pancreatitis via Amino Acid Metabolism-Mediated Macrophage Infiltration. Cellular and Molecular Gastroenterology and Hepatology. 2026; 20: 101777. https://doi.org/10.1016/j.jcmgh.2026.101777

[38] Gao T, Zhang H, Xu Y, He G, Ma H, Zheng C, et al. HIF-1α Enhances Intestinal Injury and Inflammation in Severe Acute Pancreatitis Through NLRP3 Inflammasome Activation. Digestive Diseases and Sciences. 2025; 70: 1813–1823. https://doi.org/10.1007/s10620-025-08926-y

[39] Xie X, Yang P, Wang S, Xu X, Wang L, Li P, et al. Rhaponticin alleviates pancreatic acinar cell necrosis by attenuating oxidative stress via modulation of the HIF-1α signaling pathway. Redox Report: Communications in Free Radical Research. 2026; 31: 2663628. https://doi.org/10.1080/13510002.2026.2663628

[40] Liu Y, Cui H, Mei C, Cui M, He Q, Wang Q, et al. Sirtuin4 alleviates severe acute pancreatitis by regulating HIF-1α/HO-1 mediated ferroptosis. Cell Death & Disease. 2023; 14: 694. https://doi.org/10.1038/s41419-023-06216-x

[41] Abou-Assi S, O'Keefe SJD. Nutrition support during acute pancreatitis. Nutrition (Burbank, Los Angeles County, Calif.). 2002; 18: 938–943. https://doi.org/10.1016/s0899-9007(02)00991-7

[42] Hu Q, Hu Y, Tan C, Yang Y, Su H, Huang Z, et al. Acute pancreatitis: mechanisms and therapeutic approaches. Signal Transduction and Targeted Therapy. 2026; 11: 15. https://doi.org/10.1038/s41392-025-02394-6

[43] Gukovskaya AS, Gorelick FS, Groblewski GE, Mareninova OA, Lugea A, Antonucci L, et al. Recent Insights Into the Pathogenic Mechanism of Pancreatitis: Role of Acinar Cell Organelle Disorders. Pancreas. 2019; 48: 459–470. https://doi.org/10.1097/MPA.0000000000001298